Journal of Thermal Analysis and Calorimetry (2022) 147:11921–11930
https://doi.org/10.1007/s10973-022-11393-6

Synthesis of magnetite nanoparticles coated with polyvinyl alcohol for hyperthermia application

Mohamed S. A. Darwish[1] · L. M. Al-Harbi[2] · Ahmed Bakry[3]

Received: 8 October 2021 / Accepted: 4 May 2022 / Published online: 4 June 2022

Abstract

One of the main challenges in hyperthermia treatment is how to improve the heating performance of nanoparticles with high specific loss power (SLP). To tackle this challenge, magnetite nanoparticles (MNPs) and coated magnetite nanoparticles with polyvinyl alcohol (PVA@MNPs) were fabricated via ultrasonic-assisted coprecipitation technique. The obtained nanoparticles were characterized by using FT-IR, TEM, TGA, XRD, ICP-OES, DLS, zeta potential, VSM and UV–Vis spectroscopy. The self-heating properties of the MNPs and PVA@MNPs were studied under alternating magnetic strength, frequency and induction time. MNPs and PVA@MNPs showed that the nanoparticles have a nearly spherical shape ranging between 12.3 ± 3.2 and 10 ± 2.5 nm, respectively. The higher value of zeta potentials of PVA@MNPs (− 11.49 mV) implies that the nanoparticle may show good stability in aqueous solutions. The magnetization saturation values were 41.98 and 45.08 emu g^{-1} for MNPs and PVA@MNPs, respectively. The prepared nanoparticles showed small coercivity and a remanence magnetization due to the soft magnetic nature of the prepared nanoparticles. The highest SLP value was 163.81 W g^{-1} for PVA@MNPs, while the lowest SLP value was 4.84 W g^{-1} for MNPs under the same magnetic field condition. The presence of PVA shell improved the particle stability and the magnetization for PVA@ MNPs. This successfully caused an improvement in the heating performance and magnetic hyperthermia as well. These features make the prepared PVA@MNPs in this study applicable as hyperthermic agents for biomedical applications.

Keywords Magnetite nanoparticles · Hyperthermic agents · Hyperthermia treatment · Biomedical applications

Introduction

Iron oxide nanoparticles (IONPs) have been applied widely in medical applications due to their good biocompatibility and hyperthermic characteristics [1–7]. In particular, one of the extremely advanced techniques with IONPs is magnetic hyperthermia. In this technique, the thermal energy is generated by using an alternating magnetic field (AMF) to destroy cancer cells [8]. IONPs that can elevate the temperature of the target tissues above 43 °C are appropriate for hyperthermia handling [9, 10]. The therapy with IONPs having a lower dose in a short time is highly desirable for safe and convenient hyperthermia applications [1]. The specific loss power (SLP) is the energy amount that is absorbed by IONPs mass under AMF [11]. Various techniques to synthesize IONPs have been developed, including microwave-assisted, polyol route and hydrothermal processes [12–19]. However, many of the reported techniques are expensive, time-consuming and in some cases require the use of organic solvents, which are highly reactive and toxic to the environment. The evolution of environmentally friendly and inexpensive synthetic techniques is still a defy target [19]. Magnetic nanoparticles have large surface energy and become unstable as well as tend to aggregate [20]. The properties of IONPs surface critically influence the overall heating performance of the materials [20–22]. It is important to know the particle size of IONPs because the reductions in magnetic size can decrease the heating efficiency [1]. Various coating materials such as a surfactant, organic or polymers layer are usually carried out either during or after the synthesis of nanoparticles [19]. Among these materials, polyvinyl alcohol (PVA) is

✉ Mohamed S. A. Darwish
msa.darwish@gmail.com

[1] Egyptian Petroleum Research Institute, 1 Ahmed El-Zomor Street, El Zohour Region, Nasr City, Cairo 11727, Egypt

[2] Chemistry Department, Faculty of Science, King Abdul-Aziz University, P.O. Box 80203, Jeddah 21589, Saudi Arabia

[3] Chemistry Department, Faculty of Science, Helwan University, Ain Helwan, Cairo 11795, Egypt

frequently used. PVA is a hydrophilic material and is applied in medical applications. It has a good biocompatibility, low tendency for protein adhesion and low toxicity [22]. For instance, PVA was used in the assessment of human brain tumors [22]. The introduction of PVA layer on IONPs surface can shield the magnetic iron oxide core from oxidation by the harsh chemical environment or by physiological body fluid. Besides, this enhances the colloidal stability of nanoparticles and their compatibility in the physiological environment. The suitability of IONPs for biomedical applications is attributed to their biocompatibility and non-toxicity [23]. Hence, the selection of the coating material and coating procedure should be done carefully to avoid any side effects on the biocompatibility of IONPs. Hence, this study aims at synthesizing IONPs with a high heating performance by an environmentally friendly (without surfactant or organic solvent) and a facile (at room temperature with non-expensive materials) procedure. Therefore, the preparations of coated magnetite nanoparticles with polyvinyl alcohol (PVA@MNPs) by using an ultrasonic-assisted coprecipitation process were introduced in this work. The properties of the MNPs and PVA@MNPs including the particle size, surface charge, morphology, elemental analysis and magnetic behaviors were investigated. Besides, the heating performance was studied concerning the magnetic strength, frequency and time of induction.

Experimental work

Materials

Iron (III) chloride hexahydrate ($FeCl_3{\cdot}6H_2O$), iron (II) chloride tetrahydrate ($FeCl_2{\cdot}4H_2O$), ammonium hydroxide (26%) and polyvinyl alcohol (PVA, Mw 30–70 kDa) were bought from Sigma-Aldrich, Germany.

Fabrication of iron oxide nanoparticles

Fabrication of bare MNPs

Calculated amounts of $FeCl_3{\cdot}6H_2O$ (5.4 g, 0.009 mol) and $FeCl_2{\cdot}4H_2O$ (1.9 g, 0.019 mol) were solubilized in 150 mL distilled water (DW). The solution mixed well by a mechanical stirrer for 30 min, and the temperature was increased to 70 °C. Ammonium hydroxide (6 mL, 6.6 mol) was added, producing a deep black magnetite nanoparticle precipitate. MNPs were separated magnetically, washed with DW and dried till the powder is obtained.

Fabrication of PVA@MNPs

PVA (0.5 g, 0.0071 mol) was solubilized in 50 mL of DW and then sonicated with US bath (28 kHz) for 30 min at room temperature. Then, a calculated amount of freshly prepared MNPs (1.5 g) was dispersed in the above solution and sonicated continuously in the ultrasonic bath (28 kHz) for further 60 min at room temperature. The prepared PVA@MNPs were separated magnetically, washed with DW and dried till the powder is obtained.

Characterizations

The surface charge and the size distribution were done using a Zeta-potential and Particle Size Analyzer (ELSZ-2000; Photal Otsuka Electronics, Osaka, Japan). X-ray diffraction (XRD) was performed with a Pan Analytical Model X'Pert Prob equipped with CuKα radiation ($\lambda = 0.1542$ nm). Fourier transform infrared spectroscopy (FT-IR) was performed using the Tensor 27 Infrared Spectrometer (Bruker, USA); Thermogravimetric Analysis (TGA) was measured by TA instruments Q500. TEM images were obtained through (Tecnai G2S Twin; Philips, USA) at 300 keV. The iron content in MNPs and PVA@MNPS was determined by using an inductively coupled plasma optical emission spectroscopy (ICP-OES; Optima 8300, PerkinElmer, Waltham, MA, USA). The magnetic behavior was investigated using a vibrating sample magnetometer (VSM; Lake Shore 7400 series; Lake Shore Cryotronics, USA). SLP was examined for the hyperthermia system by using Eq. 1. To investigate and optimize the heating effects, the SLP values were obtained by employing different five magnetic field conditions. Frequency (f) and magnetic field (H): (a) $f = 106.6$ kHz and $H = 20$ kA m^{-1}, (b) $f = 159.8$ kHz and $H = 13.5$ kA m^{-1}, (c) $f = 269.9$ kHz and $H = 13.5$ kA m^{-1}, (d) $f = 381.6$ kHz and $H = 12.7$ kA m^{-1}, and e) $f = 614.4$ kHz and $H = 9.5$ kA m^{-1}.

$$\mathrm{SLP} = \left(C_p/m\right) \times (\mathrm{d}T/\mathrm{d}t) \quad (1)$$

where $\mathrm{d}T/\mathrm{d}t$ is temperature per time. Cp is 4.184 J g^{-1} °C and m is iron mass.

Results and discussion

Properties of nanoparticles

Controlling the size and chemical compositions of MNPs is critical to improving their magnetic properties that effectively lead to enhancing their heating efficiency. The effect of coating MNPs with PVA using an ultrasonic-assisted coprecipitation method on the nanoparticles properties was investigated. The morphology and nanoparticles

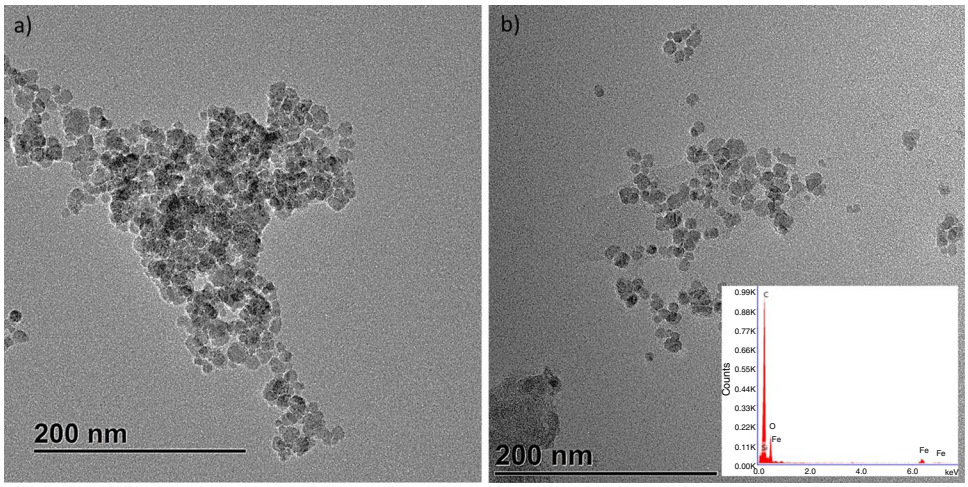

Fig. 1 TEM images and EDAX for **a** MNPs and **b** PVA@MNPs

size were studied using TEM (Fig. 1). MNPs and PVA@MNPs showed that the nanoparticles have a nearly spherical shape ranging between 12.3 ± 3.2 and 10 ± 2.5 nm, respectively. Some nanoparticles created clusters; a comparable behavior was detected by Kurchania [22]. The observed aggregation of MNPs is due to the presence of rising surface energy and magnetic dipole–dipole influence [6]. Without protective shell and aerobic condition within the preparation had promoted the hydrophobic interaction. The particles become aggregated to great clusters, resulting in growing size. This detrimental aggregation can be reduced by the introduction of a shell layer of surfactant, organic or polymer layer. The layer serves as a shielding agent to stabilize and control the size [18]. PVA@MNPs exhibited less agglomeration behavior than MNPs. The incorporation of a thin PVA layer in the structure of NP leads to enhance the mono-disperse behaviors. PVA coating provides the benefit of boost the repulsion energy to balance the magnetic and van der Waals interaction [6]. The enhanced particle dispersion for PVA@MNPs is predicted to influence the nanoparticle's heating performance. The elemental analysis and chemical characterization for PVA@MNPs were studied by an energy-dispersive spectroscopy (TEM-EDAX) (the inset in Fig. 1b). It showed the characteristic peaks at 0.6, 6.5 and 7 keV correspond to Fe atom, which confirms the formation of IONPs. Also, the presence of PVA was confirmed by the energy peak for C and O atoms at 0.2 and 0.5 keV, respectively. TEM-EDAX confirmed the presence of PVA and Fe in the prepared nanostructure of PVA@MNPs. The iron content in the fabricated nanoparticles was measured using ICP-OES. It was observed that the mass percentages of Fe in MNPs and PVA@MNPs nanoparticles were 50.8% and 66.6%, respectively, which is expected to influence their heating efficiency properties.

The mean size and the size distribution of the particles were investigated using DLS. The results of DLS analyses for MNPs and PVA@MNPs are shown in Fig. 2. The observed mean hydrodynamic sizes for MNPs and PVA@MNPs were 237 nm and 222.4 nm, respectively. MNPs show a wider size distribution than PVA@MNPs. DLS shows statistical values about the hydrodynamic size of nanoparticles. The performance of DLS analysis depends on many factors as the particle size, sample shape, concentration of the sample, polydispersity and surface properties. Scattering may not be sufficient to have a suitable detection for diluted samples. Otherwise, multiple scattering can occur for concentrated samples. The existence of the larger particles will take over the light scattering indicative and face the existence of the smaller one [24, 25].

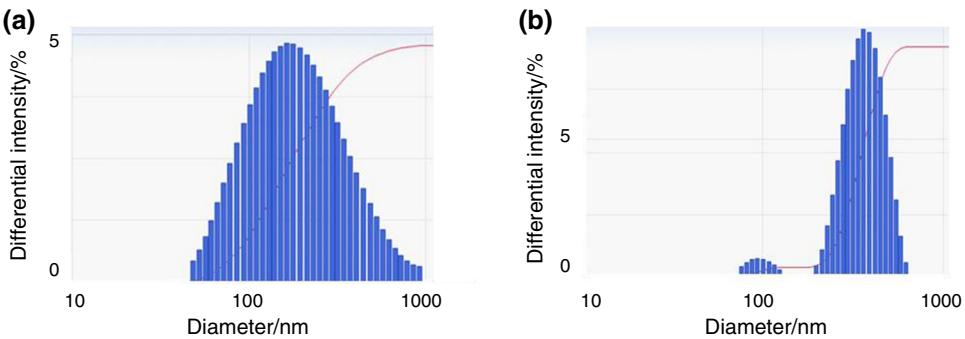

Fig. 2 DLS for **a** MNPs and **b** PVA@MNPs

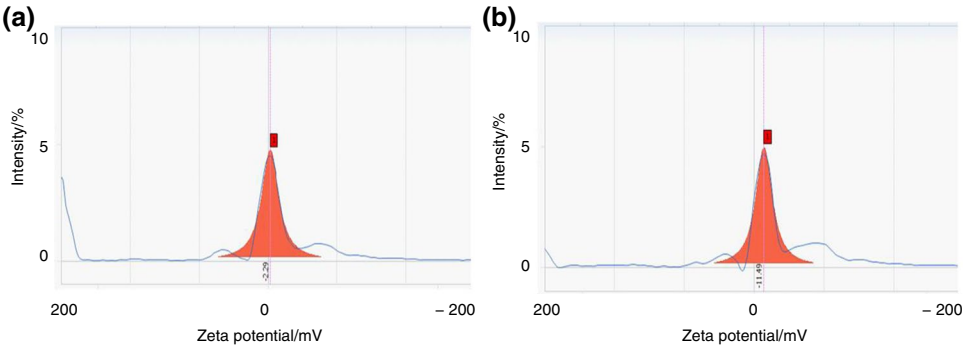

Fig. 3 Zeta potential for **a** MNPs and **b** PVA@MNPs

A zeta potential (ζ) of the fabricated nanoparticles was studied, which is predictive of the colloidal stability and aggregation of nanoparticles (Fig. 3). Nanoparticles' stability is very important for biomedical applications to achieve expectable and consistent outcomes [26]. The low value of zeta potential of MNPs (− 2.29 mV) implies that the nanoparticle may show poor stability in aqueous solutions. Low zeta potential values (0 to ± 5 mV) will improve Van der Waals interparticle attractions and causes rapid coagulation and flocculation of nanoparticles [22]. On the other hand, the higher value of zeta potentials of PVA@MNPs (− 11.49 mV) implies that the nanoparticle may show good stability in aqueous solutions. There is a specific zeta potential value (≈ ± 30 mV) that determines the stability of nanoparticles. At this value, high electrostatic repulsive forces between the nanoparticles occur [26]. Zeta potential with negative value was detected on PVA-magnetic nanoparticles surface by Demerlis et al. It shows that the sample reveal reveals sensible colloidal constancy regarding the electrostatic repulsion [27]. PVA@MNPs samples obtained in this work exhibit more negative values than those reported by others. For instance, a zeta potential value of − 10.9 ± 3.5 mV was reported for PVA shelled Fe_3O_4 by Vilos et al. [28].

The type of magnetic phase and the estimated average grain size were studied using XRD. The peaks along (440), (511), (422), (400), (311) and (220) lattice planes correspond to the standard pattern (reference code: 98-015-8742) for the dominant magnetite nanoparticles phase (Fe_3O_4). However, the peaks along (104), (113), (116) and (024) planes correspond to α- Fe_2O_3 (Fig. 4) [29]. Magnetite phase easily oxidizes at an atmospheric condition in the lack of an encapsulating oxygen block. The peaks for PVA@MNPs were weak and to some extent broad, probable due to disorder and small crystallite effects. The broadening of peaks relies on various parameters such as the instrumental effect, strain effect and finite crystallite size. The size of nanoparticles was estimated from the Debye–Scherrer equation (Eq. 2).

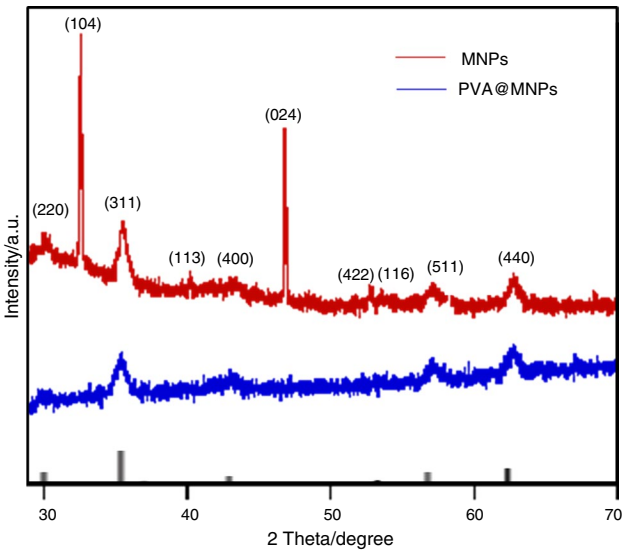

Fig. 4 XRD for MNPs and PVA@MNPs

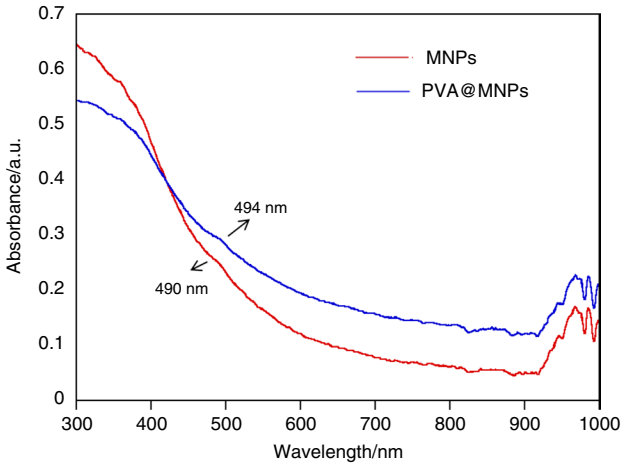

Fig. 5 Optical spectra for MNPs and PVA@MNPs

$$D_p = \frac{K\lambda}{\beta\cos\theta} \quad (2)$$

where D_p is the grain size, β is the FWHM, λ is the 1.5406 Å, K is the Scherrer constant, and θ is the Bragg angle.

The observed grain sizes for MNPs and PVA@MNPs were 11.7 nm and 9.8 nm, respectively.

The optical absorbance spectra of MNPs and PVA@MNPs were studied using UV–Vis spectroscopy (Fig. 5). The absorption peak for iron-oxides NPs is generally at the range of 300–600 nm. MNPs exhibited thermally promote electronic transitions regard to intervalence charge carriage. They showed absorption within the visible and near-IR region [29]. Our nanoparticles exhibited a broad absorption range from 300 to 600 nm in the range of visible wavelength. The MNPs peak was found to be at 490 nm. However, PVA@MNPs showed a shift in the absorption peak and appeared at 494 nm matched to the d-d transition for Fe^{3+} [30]. The optical absorbance spectra of the magnetite phase in the prepared nanoparticle were detected.

The FT-IR was used to detect the existing functional groups on the MNPs surface as shown in Fig. 6. The absorption band observed near 580 cm^{-1} confirmed that the Fe–O bond is present in the synthesized MNPs and PVA@MNPs. The absorption band at 3388 cm^{-1} corresponded to the stretching vibrations of –OH groups in the PVA@MNPs [22]. The additional bands close to 2860 and 1090 cm^{-1} were attributed to C–H stretching vibrations and the –O–C stretching vibrations, respectively. Therefore, the FT-IR results confirmed that the PVA polymer layer existed on the surfaces of the synthesized MNPs.

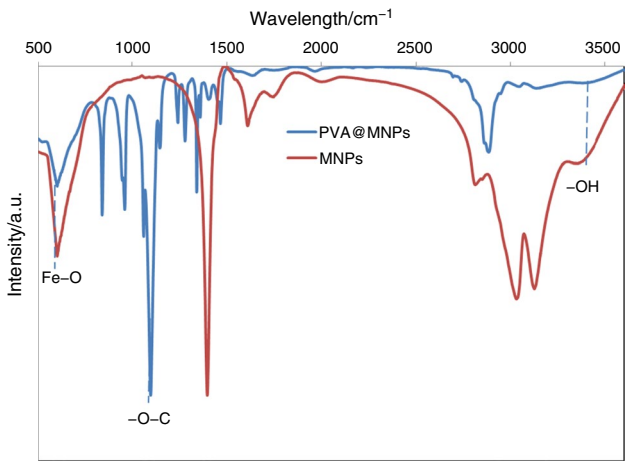

Fig. 6 FT-IR for MNPs and PVA@MNPs

The thermal stability of the MNPs and PVA@MNPs was evaluated using TGA. The TG-DTG curves are presented in Fig. 7a, b. The first stage of mass loss, observed at the range of 100–200 °C, was attributed to the loss of water. The mass loss at 200 °C is about 22.12%. A second mass loss, noted in the temperature range of 200–400 °C, was attributed to the decomposition of the polymer. Above 200 °C, the PVA shell material decomposes. According to the results, PVA@MNPs exhibited the onset of decomposition at a temperature lower than that observed for the uncoated MNPs. The decomposition was attributed to the dehydration reaction of –OH groups in PVA chains and subsequent degradation of PVA-releasing CO_2 gas. The mass loss at 400 °C is about 41.2%. This was followed by a final stage, at the temperature range of 400–800 °C. The thermal stability of the synthesized nanoparticles became almost unwavering above 400 °C. The uncoated iron oxide nanoparticles (MNPs) exhibited the highest thermal stability. The mass of the final residue was 60.9% and 56.6% for the MNPs and PVA@MNPs, respectively. This is because of the existence of the inorganic element that is expected to affect the heating efficiency behavior of the nanoparticles.

Magnetic properties for MNPs and PVA@MNPs were performed using VSM at room temperature (Fig. 8). The magnetic behavior of uncoated and PVA-coated MNP showed soft magnetic property with small coercivity (Hc) 7.8 G and remanence (M_r) 4.2 emu g^{-1}. If the MNP size is preserved beneath a critical size, the MNPs head to promote as a single magnetic domain frame. At the

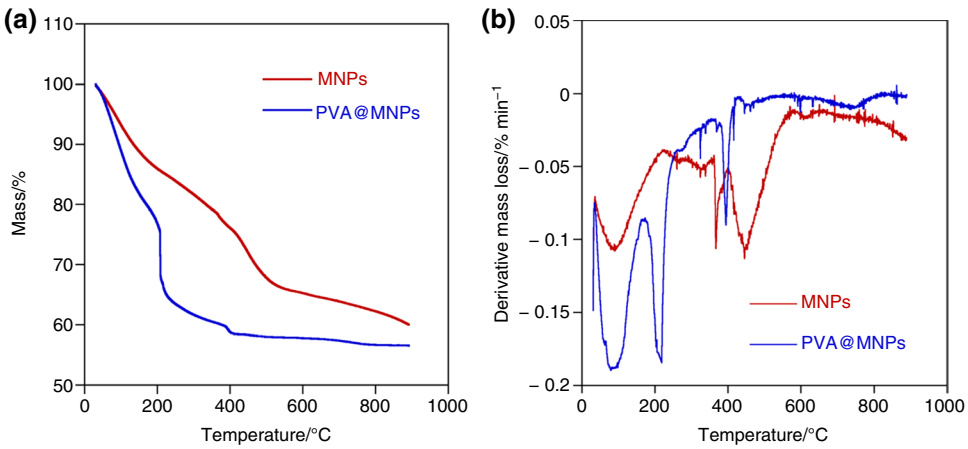

Fig. 7 TG and DTG curves for MNPs and PVA@MNPs

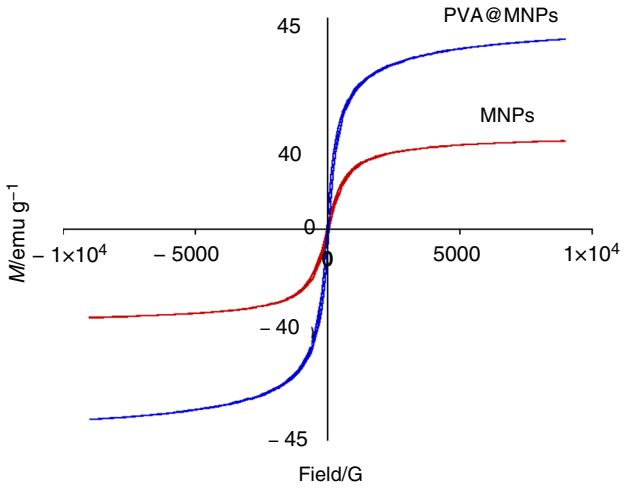

Fig. 8 VSM for MNPs and PVA@MNPs

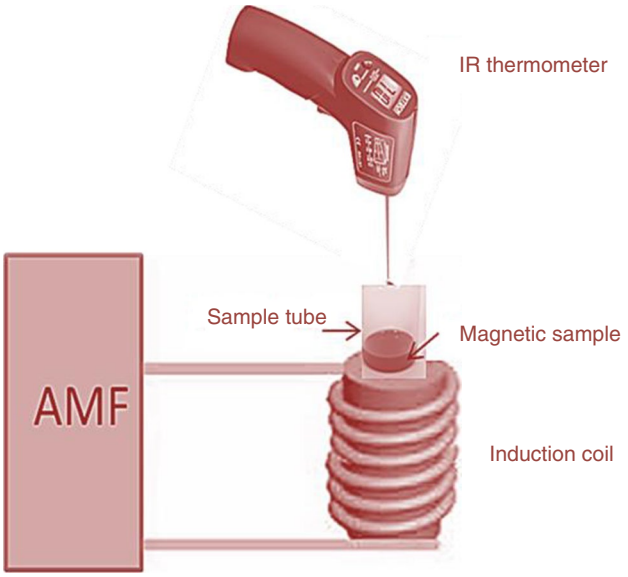

Fig. 9 Magnetic induction heating system

smallest size, MNPs display superparamagnetic attitudes under standard conditions. The magnetization saturation (M_s) values were 41.98 and 45.08 emu g^{-1} for MNPs and PVA@MNPs, respectively (Fig. 8). The slight increase in the *Ms* value of PVA@MNPs is likely to refer to the contact potential prompt at the Fe_3O_4-PVA interface [31]. The increase in magnetic saturation values of polymer-coated samples was probably attributed to the contact potential induced at the iron-polymer interface [31]. Fe_3O_4 and γ Fe_2O_3 (20 to 30 nm) were coated with polyaniline. Polyaniline coating exhibited an increase in saturation magnetization by 2 emu g^{-1}. This enhanced magnetization is found to be an interfacial phenomenon resulting from a contact potential. Recently, Mol et al. confirm a similar observation that the *Ms* of uncoated Fe_3O_4 is less than for polymer-coated Fe_3O_4. *Ms* of PANI-coated and polypyrrole-coated Fe_3O_4 nanoparticles was 55 and 52 emu g^{-1}, respectively. However, *Ms* was 51 emu g^{-1} for Fe_3O_4, which is less than for polymer-coated Fe_3O_4 due to surface/interfacial magnetism [32]. These observed behaviors were in agreement with those reported in the literature and thereby confirmed an increase in saturation magnetization value PVA@MNPs [31, 32]. There have been several reports on the decrease in *Ms* values of composites as magnetite nanoparticles are incorporated into a nonmagnetic polymer matrix [22, 29, 33, 34]. The saturation magnetization value for Fe_3O_4-PVA is 0.52 emu g^{-1} [33]. The hysteresis loop shows that Fe_3O_4-PVA was superparamagnetic with no coercivity at room temperature. The *Ms* value 30 emu g^{-1} for PVA-magnetite nanoparticles was measured by Kayal et al. [34]. The particles are superparamagnetic at room temperature which is useful in drug delivery as they do not retain magnetization before and after exposure to an external magnetic field. The *Ms* value 56.41 emu g^{-1} for PVA-magnetite nanoparticles was measured by Kurchania et al. [22]. It shows that the sample reveals superparamagnetic behavior with no remanence and coercivity. A magnetite/PVA nanocomposite film shows a typical superparamagnetic behavior at room temperature without any hysteresis loop since the remanence and coercivity are negligible. The saturation magnetization *Ms* at room temperature was 8.1 emu g^{-1} [29].

Hyperthermia performance

Under an alternative magnetic field, magnetic IONPs were able to generate localized heat energy as a thermal source (Fig. 9) [35–42]. For effective hyperthermia application, IONPs should satisfy a small particle size and a high *Ms*. This increase in temperature is the basis in cancer therapy applications by magnetic induction heating behavior [5–7].

In this study, the heating efficiency and SLP values were studied by employing five different magnetic field conditions to optimize the heating effects (Figs. 10, 11). As shown in Figs. 10, 11, the temperature elevated with time nearly in a linear way (a quasi-adiabatic regime). After that, the increase in temperature slowed down progressively till reaching a saturation region. At this region, the temperature did not increase any longer and reached thermal equilibrium [33]. The samples became heated faster and the heating rate rose by increasing frequency as demonstrated in Fig. 10. Magnetic nanoparticles have the feature of supplying high heating performance with a lower dose by faster hyperthermia treatment. When comparing the heating efficiency of MNPs to PVA@MNPs, PVA@MNPs were found to show

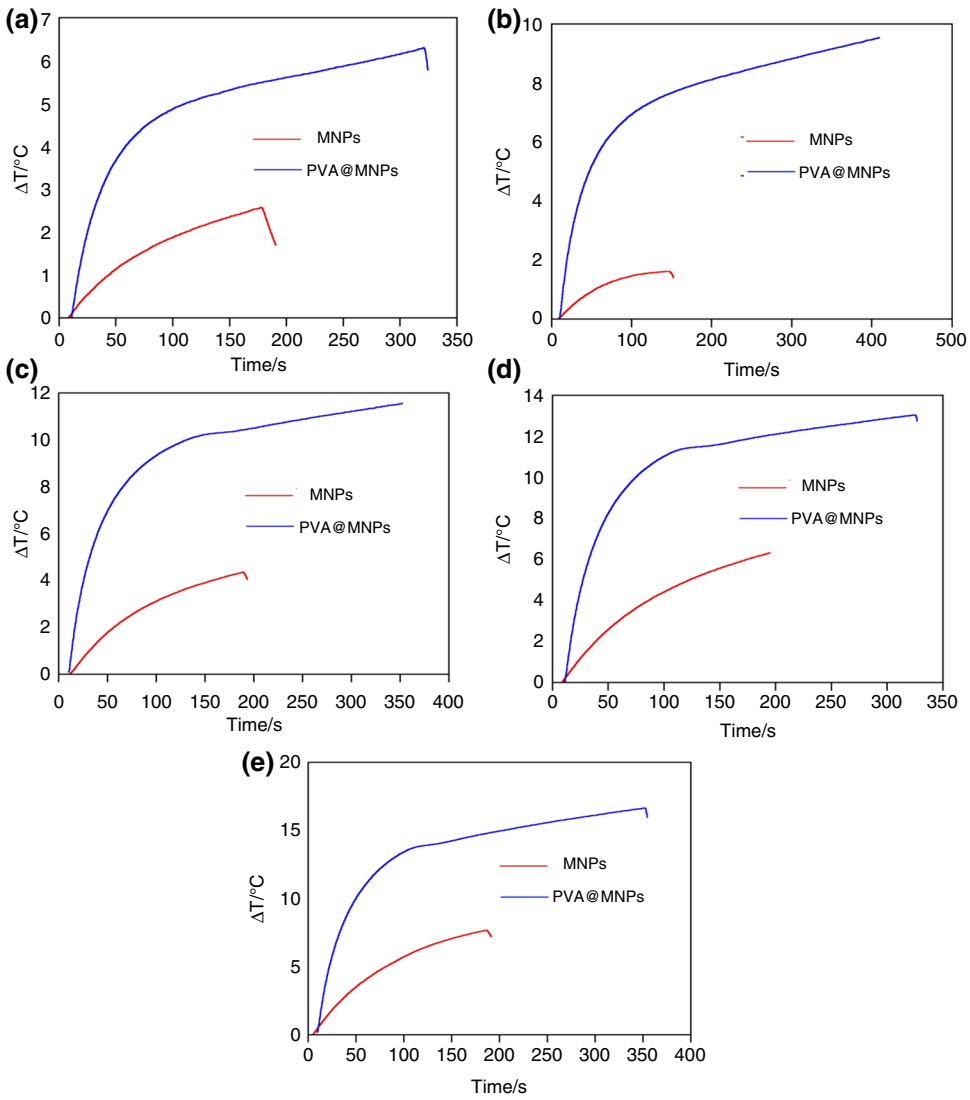

Fig. 10 Heating efficiency for MNPs and PVA@MNPs at the conditions: **a** $f = 106.6$ kHz and $H = 20$ kA m^{-1}, **b** $f = 159.8$ kHz and $H = 13.5$ kA m^{-1}, **c** $f = 269.9$ kHz and $H = 13.5$ kA m^{-1}, **d** $f = 381.6$ kHz and $H = 12.7$ kA m^{-1} and **e** $f = 614.4$ kHz and $H = 9.5$ kA m^{-1}

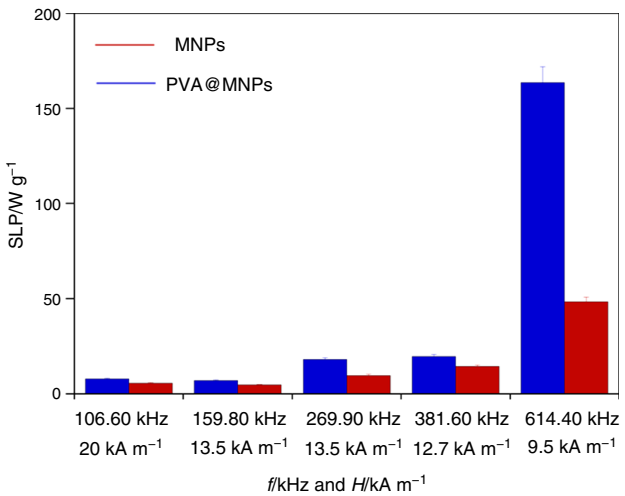

Fig.11 Specific loss power (SLP) of MNPs and PVA@MNPs

the highest efficiency. The enhanced stability, uniform particle dispersion and high magnetization saturation for PVA@MNPs improved the heating performance effectively.

The heating efficiency of the MNPs and PVA@MNPs was investigated under a magnetic field strength (13.5 kA m^{-1}) with different frequencies in the range from 159.8 to 269.9 kHz, as shown in Fig. 10b–c. For PVA@MNPs nanoparticles, the heating rate increased and the temperature elevations were 7.1 °C and 9.5 °C after 200 s with 159.8 kHz and 269.9 kHz, respectively. As a result, the heating efficiency increased as the frequency increased under a constant magnetic field strength. For effective hyperthermia treatment, the temperature of cancer cells should be elevated 6–8 °C to reach (43–45 °C).

The heating performance is quantified by the parameter SLP, which is equal to the dissipated power divided by the magnetic material density. SLP varies linearly with the product of frequency, f, and the square of the magnetic field (H^2).

The heating performance curves show temperature elevation with time [35]. For human exposure and biosafety, the product of strength and frequency of the AMF must be maintained below a threshold safety value (5×10^9 A m^{-1} s^{-1}). The heating efficiency of the fabricated particles in this study could be enhanced with $f = 614.4$ kHz and $H = 9.5$ kA m^{-1}. A comparison of SLP of MNPs and PVA@MNPs nanoparticles is shown in Fig. 11. Under the same magnetic field condition, PVA@MNPs showed the highest SLP with better hyperthermic response. It was found that the highest SLP value was 163.81 W g^{-1} for PVA@MNPs under magnetic conditions of frequency = 614.4 kHz and magnetic field = 9.5 kA m^{-1}. However, the lowest SLP value was 4.84 W g^{-1} for MNPs under magnetic conditions of frequency = 159.8 kHz and magnetic field = 13.5 kA m^{-1}. SLP is affected by the saturation magnetization, as shown by Eq. 3 for SLP. Modulation of the shape and size of IONPs can tune their magnetic properties, induce saturation magnetization and further enhance magnetic hyperthermia properties.

$$\mathrm{SLP} = \frac{\pi \cdot \mu_0 \cdot \chi''(f) \cdot H^2 \cdot f}{\rho_{\mathrm{MNPs}} \cdot \phi}, \quad \chi''(f) = \frac{\mu_0 M_s^2 V}{3 k_B T} \frac{\omega \tau_R}{\left(1 + \omega^2 \tau_R^2\right)} \tag{3}$$

where f is the frequency, H is the field strength, ρ_{MNPs} is the density of nanoparticles, ϕ is the volume fraction, μ_0 is the permeability, and χ'' is the susceptibility. M_s is the saturation magnetization, V is the volume of the MNPs, $\omega = 2\pi f$ is the sweep rate of AMF, τ_R is the time of relaxation, and k_B is Boltzmann's constant.

The heating efficiency is affected by various factors, such as the magnetic field condition, size of the nanoparticles, magnetic behaviors and coated layer. Hence, the magnetic nanoparticles should be prepared with a proper method to reach the target temperature [36, 37].

The single-domain size from 20 to 70 nm along with a narrow size distribution is reported to improve the loss of power value [38]. The reported values for SLP in the literature are 10–100 W g^{-1} for magnetic field conditions of $H = 10$ kA m^{-1} and $f \approx 400$ kHz [39]. Nigam et al. have reported magnetite nanoparticles coated with citrate that showed a high SLP to reach the target temperature (43 °C) in a short time with increases of the magnetic field [40]. High SLP (150 W g^{-1}) was reached under magnetic field condition of $H = 20$ mT and $f = 205$ kHz [41]. The SLP value shifted from almost zero for 4.1 and 6.7 nm MNPs to ~ 76 W g^{-1} for 35 nm rhamnose-coated Fe_3O_4 MNPs [43]. Magnetite nanoparticles @ chitosan (15 nm) showed (SLP = 119 W g^{-1}) higher than uncoated magnetite nanoparticles. The enhancement in the particle dispersion is because of the presence of the hydrophilic shell layer [42]. The heat dissipation has resulted fundamentally from the magnetic moment's relaxation termed as Neel relaxation and Brownian relaxation [35–42]. In Neel relaxation, there is opposition by the particle's crystalline structure, resulting in heat generation. In Brownian relaxation, the heat is created from the physical rotation of particles within the medium. It results in SLP value reduction. These relaxations also rely upon magnetic particles size. In general, Neel relaxation dominates when nanoparticles are less than 20 nm [44]. The diversity in the heating performance of polymer-coated MNPs is related to individual NPs relaxation into the polymer shell which results in a growing in heating performance than uncoated MNPs [32]. PVA@MNPs (10 ± 2.5 nm) prepared via ultrasonic-assisted coprecipitation process, in the current study, exhibited a high SLP value (163.81 W g^{-1}). This suggests that these PVA@MNPs could be used for hyperthermia treatments.

Conclusions

Magnetite nanoparticles coated with polyvinyl alcohol were fabricated successfully through an ultrasonic-assisted coprecipitation technique. The dispersion of MNPs and the magnetization value (45.08 emu g^{-1}) were enhanced after coating with PVA shell. The presence of PVA beneficially improves the heating efficiency and hyperthermia properties as well. Under high frequency, the maximum SLP could be obtained with PVA@MNPs. PVA@MNPs showed the highest SLP value (163.81 W g^{-1}), while MNPs showed the lowest one (4.84 W g^{-1}). Accordingly, the self-heating properties of the prepared PVA@MNPs show promise in hyperthermia applications.

Author contributions MSAD and AB performed the synthesis and characterization of composites and wrote the majority of the manuscript. LMA-H participated in writing the manuscript, supervised the conceptual framework and corrected the manuscript. All authors read and approved the final manuscript.

Funding Open access funding provided by The Science, Technology & Innovation Funding Authority (STDF) in cooperation with The Egyptian Knowledge Bank (EKB).

Declarations

Conflict of interest The authors declare no conflict of interest.

References

1. Rytov RA, Bautin VA, Usov NA. Towards optimal thermal distribution in magnetic hyperthermia. Sci Rep. 2022;12:3023. https://doi.org/10.1038/s41598-022-07062-1.
2. Vasquez ES, Prehn EM, Walters KB. Assessing magnetic iron oxide nanoparticle properties under different thermal treatments. J Therm Anal Calorim. 2021;143:35–46. https://doi.org/10.1007/s10973-019-09195-4.
3. Healy S, Bakuzis AF, Goodwill PW, Attaluri A, Bulte JWM, Ivkov R. Clinical magnetic hyperthermia requires integrated magnetic particle imaging. Wiley Interdiscip Rev Nanomed Nanobiotechnol. 2022. https://doi.org/10.1002/wnan.1779.
4. Zhang Y, Gao X, Yan B, Wen N, Lee WSV, Liang XJ, Liu X. Enhancement of CD8+ T-Cell-mediated tumor immunotherapy via magnetic hyperthermia. ChemMedChem. 2022;17:e202100656. https://doi.org/10.1002/cmdc.202100656.
5. Narayanaswamy V, Al-Omari IA, Kamzin AS, Issa B, Obaidat IM. Tailoring interfacial exchange anisotropy in hard-soft core-shell ferrite nanoparticles for magnetic hyperthermia applications. Nanomaterials. 2022;12:262. https://doi.org/10.3390/nano12020262.
6. Bhardwaj A, Jain N, Parekh K. Investigating the effect of outer layer of magnetic particles on cervical cancer cells HeLa by magnetic fluid hyperthermia. Cancer Nano. 2021;12:7. https://doi.org/10.1186/s12645-021-00076-w.
7. Ganapathe LS, Mohamed MA, Mohamad Yunus R, Berhanuddin DD. Magnetite (Fe_3O_4) nanoparticles in biomedical application: from synthesis to surface functionalisation. Magnetochemistry. 2020;6:68. https://doi.org/10.3390/magnetochemistry6040068.
8. Rajan A, Sharma M, Sahu NK. Assessing magnetic and inductive thermal properties of various surfactants functionalised Fe_3O_4 nanoparticles for hyperthermia. Sci Rep. 2020;10:15045. https://doi.org/10.1038/s41598-020-71703-6.
9. Wang J, Zhang B, Wang L, Wang M, Gao F. One-pot synthesis of water-soluble superparamagnetic iron oxide nanoparticles and their MRI contrast effects in the mouse brains. Mater Sci Eng C Mater Biol Appl. 2015;48:416–23. https://doi.org/10.1016/j.msec.2014.12.026.
10. Eskandari MJ, Hasanzadeh I. Size-controlled synthesis of Fe_3O_4 magnetic nanoparticles via an alternating magnetic field and ultrasonic-assisted chemical co-precipitation. Mater Sci Eng B. 2021;266:115050. https://doi.org/10.1016/j.mseb.2021.115050.
11. Coffel J, Nuxoll E. Magnetic nanoparticle/polymer composites for medical implant infection control. J Mater Chem B. 2015;3:7538–45. https://doi.org/10.1039/C5TB01540E.
12. Barvinschi P, Stefanescu O, Dippong T, Sorescu S, Stefanescu M. CoFe2O4/SiO2 nanocomposites by thermal decomposition of some complex combinations embedded in hybrid silica gels. J Therm Anal Calorim. 2013;112:447–53. https://doi.org/10.1007/s10973-012-2704-9.
13. Dippong T, Levei EA, Cadar O, Goga F, Borodi G, Barbu-Tudoran L. Thermal behavior of $Co_xFe_{3-x}O_4/SiO_2$ nanocomposites obtained by a modified sol–gel method. J Therm Anal Calorim. 2017;128:39–52. https://doi.org/10.1007/s10973-016-5930-8.
14. Ştefănescu M, Dippong T, Stoia M, Ştefănescu O. Study on the obtaining of cobalt oxides by thermal decomposition of some complex combinations, undispersed and dispersed in SiO_2 matrix. J Therm Anal Calorim. 2008;94:389–93. https://doi.org/10.1007/s10973-008-9111-2.
15. Dippong T, Levei EA, Borodi G, Goga F, Tudoran LB. Influence of Co/Fe ratio on the oxide phases in nanoparticles of $Co_xFe_{3-x}O_4$. J Therm Anal Calorim. 2015;119:1001–9. https://doi.org/10.1007/s10973-014-4280-7.
16. Liu Z, Lanier OL, Chauhan A. Poly (vinyl alcohol) assisted synthesis and anti-solvent precipitation of gold nanoparticles. Nanomaterials. 2020;10:2359. https://doi.org/10.3390/nano10122359.
17. Li S, Zhang W, Chen F, Chen R. One-pot hydrothermal synthesis of Pd/Fe_3O_4 nanocomposite in HEPES buffer solution and catalytic activity for Suzuki reaction. Mater Res Bull. 2015;66:186–91. https://doi.org/10.1016/j.materresbull.2015.02.042.
18. Anbarasu M, Anandan M, Chinnasamy E, Gopinath V, Balamurugan K. Synthesis and characterization of polyethylene glycol (PEG) coated Fe_3O_4 nanoparticles by chemical co-precipitation method for biomedical applications. Spectrochim Acta A. 2015;135:536–9. https://doi.org/10.1016/j.saa.2014.07.059.
19. Darwish MSA, Stibor I. Pentenoic acid-stabilized magnetic nanoparticles for nanomedicine applications. J Dispers Sci Technol. 2016;37:1793–8. https://doi.org/10.1080/01932691.2016.1140584.
20. Ghazanfari MR, Kashefi M, Shams SF, Jaafari MR. Perspective of Fe_3O_4 nanoparticles role in biomedical applications. Biochem Res Int. 2016;2016:1–32. https://doi.org/10.1155/2016/7840161.
21. Darwish MSA, Bakry A, Kolek O, Martinová L, Stibor I. Electrospun functionalized magnetic polyamide 6 composite nanofiber: Fabrication and stabilization. Polym Compos. 2019;40:296–303. https://doi.org/10.1002/pc.24647.
22. Kurchania R, Sawant SS, Ball RJ. Synthesis and characterization of magnetite/polyvinyl alcohol core-shell composite nanoparticles. J Am Ceram Soc. 2014;97:3208–15. https://doi.org/10.1111/jace.13108.
23. Yüksel Y. Effects of the particle size and shape of the magnetic nanoparticles on the magnetic hyperthermia and exchange bias properties. Physica B Condens Matter. 2019;575: 411689. https://doi.org/10.1016/j.physb.2019.411689.
24. Lim J, Yeap SP, Che HX, et al. Characterization of magnetic nanoparticle by dynamic light scattering. Nanoscale Res Lett. 2013. https://doi.org/10.1186/1556-276X-8-381.
25. Takahashi K, Kato H, Saito T, Matsuyama S, Kinugasa S. Precise measurement of the size of nanoparticles by dynamic light scattering with uncertainty analysis. Part Part Syst Charact. 2008;25:31–8. https://doi.org/10.1002/ppsc.200700015.
26. Kmita A, Lachowicz D, Żukrowski J, Gajewska M, Szczerba W, Kuciakowski J, Zapotoczny S, Sikora M. One-step synthesis of long term stable superparamagnetic colloid of zinc ferrite nanorods in water. Materials. 2019;12:1048. https://doi.org/10.3390/ma12071048.
27. Demerlis CC, Schoneker DR. Review of the oral toxicity of polyvinyl alcohol (PVA). Food Chem Toxicol. 2003;41:319–26.
28. Vilos C, Gutierrez M, Escobar R, Morales F, Denardin J, Velásquez L, Altbir D. Superparamagnetic poly (3-hydroxybutyrate-co-3 hydroxyvalerate) (PHBV) nanoparticles for biomedical applications. Electron J Biotechnol. 2013. https://doi.org/10.2225/vol16-issue5-fulltext-8.
29. Badawy SM, Abd E-L. Synthesis and characterizations of magnetite nanocomposite films for radiation shielding. Polym Compos. 2017;38:974–80. https://doi.org/10.1002/pc.23660.
30. Sarkar A, Biswas SK, Pramanik P. Design of a new nanostructure comprising mesoporous ZrO_2 shell and magnetite core (Fe_3O_4@$mZrO_2$) and study of its phosphate ion separation efficiency. J Mater Chem. 2010;20:4417–24. https://doi.org/10.1039/B925379C.
31. Sethulakshmi N, Sooraj V, Sajeev US, Nair SS, Narayanan TN, Joy LK, Joy PA, Ajayan PM, Anantharaman MR. Contact

potential induced enhancement of magnetization in polyaniline coated nanomagnetic iron oxides by plasma polymerization. Appl Phys Lett. 2013;103: 162414. https://doi.org/10.1063/1.4826459.
32. Mol B, Beeran AE, Jayaram PS, et al. Radio frequency plasma assisted surface modification of Fe_3O_4 nanoparticles using polyaniline/polypyrrole for bioimaging and magnetic hyperthermia applications. J Mater Sci Mater Med. 2021;32:108. https://doi.org/10.1007/s10856-021-06563-1.
33. Wang Y, Shi Z, Sun Y, Wu X, Li S, Dong S, Lan T. Preparation of amphiphilic magnetic polyvinyl alcohol targeted drug carrier and drug delivery research. Des Monomers Polym. 2020;23(1):197–206. https://doi.org/10.1080/15685551.2020.1837442.
34. Kayal S, Ramanujan RV. Doxorubicin loaded PVA coated iron oxide nanoparticles for targeted drug delivery. Mater Sci Eng C Biom Mater Sens Syst. 2010;30:484–90. https://doi.org/10.1016/j.msec.2010.01.006.
35. Piñeiro-Redondo Y, Bañobre-López M, Pardiñas-Blanco I, et al. The influence of colloidal parameters on the specific power absorption of PAA-coated magnetite nanoparticles. Nanoscale Res Lett. 2011;6:383. https://doi.org/10.1186/1556-276x-6-383.
36. Ma M, Wu Y, Zhou J, Sun Y, Zhang Y, Gu N. Size dependence of specific power absorption of Fe_3O_4 particles in AC magnetic field. J Magn Magn Mater. 2004;268:33–9. https://doi.org/10.1016/S0304-8853(03)00426-8.
37. Hergt R, Hiergeist R, Zeisberger M, Glockl G, Weitschies W, Ramirez LP, Hilger I, Kaiser WA. Enhancement of AC-losses of magnetic nanoparticles for heating applications. J Magn Magn Mater. 2004;80:358–68. https://doi.org/10.1016/j.jmmm.2004.03.034.
38. Hergt R, Dutz S. Magnetic particle hyperthermia—biophysical limitations of a visionary tumour therapy. J Magn Magn Mater. 2007;311(1):187–92. https://doi.org/10.1016/j.jmmm.2006.10.1156.
39. Hergt R, Dutz S, Muller R, Zeisberger M. Magnetic particle hyperthermia: nanoparticle magnetism and materials development for cancer therapy. J Phys Condens Matter. 2006;18:S2919. https://doi.org/10.1088/0953-8984/18/38/S26.
40. Nigam S, Barick K, Bahadur D. Development of citrate-stabilized Fe_3O_4 nanoparticles: conjugation and release of doxorubicin for therapeutic applications. J Magn Magn Mater. 2011;323:237–43. https://doi.org/10.1016/j.jmmm.2010.09.009.
41. Reyes-Ortega F, Delgado ÁV, Schneider EK, Checa Fernández BL, Iglesias GR. Magnetic nanoparticles coated with a thermosensitive polymer with hyperthermia properties. Polymers. 2018;10:10. https://doi.org/10.3390/polym10010010.
42. Shete PB, Patil RM, Thorat ND, Prasad A, Ningthoujam RS, Ghosh SJ, Pawar SH. Magnetic chitosan nanocomposite for hyperthermia therapy application: Preparation, characterization and in vitro experiments. Appl Surf Sci. 2014;288:149–57. https://doi.org/10.1016/j.apsusc.2013.09.169.
43. Lartigue L, Innocenti C, Kalaivani T, Awwad A, del Mar M, Duque S, Guari Y, Larionova J, Guérin C, Montero JL-G, Barragan-Montero V, et al. Water-dispersible sugar-coated iron oxide nanoparticles. An evaluation of their relaxometric and magnetic hyperthermia properties. J Am Chem Soc. 2011;133(27):10459–72. https://doi.org/10.1021/ja111448t.
44. Chung SH, Hoffmann A, Bader SD. Biological sensors based on Brownian relaxation of magnetic nanoparticles. Appl Phys Lett. 2004;85:2971. https://doi.org/10.1063/1.1801687.